

pubs.acs.org/acscatalysis Research Article

Carbon Dioxide Reduction with Dihydrogen and Silanes at Low-Valent Molybdenum Terphenyl Diphosphine Complexes: Reductant Identity Dictates Mechanism

Joshua A. Buss, Naoki Shida, Tianyi He, and Theodor Agapie*



Cite This: ACS Catal. 2021, 11, 13294–13302



Read Online

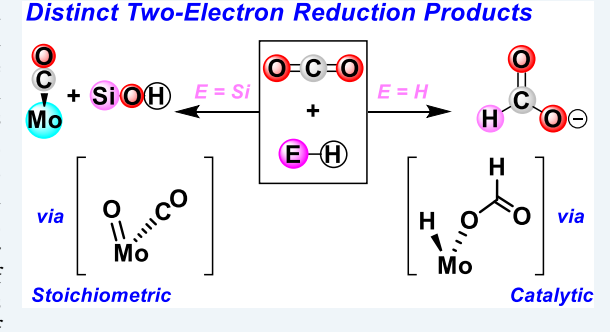
ACCESS

Metrics & More

Article Recommendations

s Supporting Information

ABSTRACT: The reaction chemistry of both silanes and hydrogen at *para*-terphenyl diphosphine-supported molybdenum complexes was explored within the context of carbon dioxide (CO₂) reduction. CO₂ hydrosilylation commonly affords reduction products via silyl acetals. However, while silyl hydride complexes were characterized in the present system, synthetic, spectroscopic, and kinetic studies suggest C–O cleavage of CO₂ occurs independently of silanes. In their presence, a putative molybdenum oxo intermediate is hypothesized to undergo O-atom transfer, yielding silanol. In contrast, hydrogenation chemistry does occur through an intermediate molybdenum dihydride capable of inserting CO₂ to yield a formate hydride complex. This process is reversible; slow deinsertion under dinitrogen affords a mixture of



molybdenum dihydride, η^2 -CO₂, and N₂ complexes. The molybdenum hydride formate species is a competent precatalyst for both CO₂ hydrogenation to formate (in the presence of lithium cations and base) and formic acid dehydrogenation to CO₂ and hydrogen (in the presence of base). Mechanistic studies of both catalytic processes are presented.

KEYWORDS: CO₂ reduction, hydrogen storage, formic acid dehydrogenation, hydrosilylation, molybdenum

1. INTRODUCTION

Carbon oxygenates (particularly carbon dioxide) represent quintessential precursors for the formation of solar fuels—renewable reservoirs of transportable energy generated via reducing equivalents sourced from sunlight. Technologies enabling this process would alleviate societal reliance on fossil fuels for dependable and stable energy. While abundant, the kinetic and thermodynamic stability of carbon dioxide (CO₂) hamper its conversion chemistry. Recent strategies to overcome these limitations employ energy-rich reactants, including high-energy electrons, Position of energy electrons, and reactive E—H bonds (boranes, silanes, energy electrons). The hydrosilylation of CO₂ can proceed in a well-defined

The hydrosilylation of CO₂ can proceed in a well-defined manner, furnishing a series of reduction products utilizing the electrons stored in Si–H bonds and driven by the formation of strong Si–O bonds. ^{12,13} Commonly, this chemistry invokes CO₂ insertion into a M–H (generated via Si–H bond activation) and subsequent silyl formate formation, which can serve as a synthon for myriad value-added chemicals. ¹⁴ Though a common byproduct in CO₂ hydrosilylation catalysis, silanol is generally formed via nucleophilic substitution reactions of silyl formates, meaning that the C–O bond of CO₂ is broken after reduction and dissociation from the metal. ¹⁵ Herein, we disclose reversible Si–H oxidative addition to low-valent molybdenum and C–O cleavage of CO₂. Silyl

hydride complexes, while proving capable of efficient CO_2 reduction to carbon monoxide (CO) and silanol, are not the species responsible for the observed C $-\mathrm{O}$ bond scission.

In conjunction with exploring CO_2 hydrosilylation chemistry, hydrogenation chemistry was targeted for comparison. Though H_2 is a potential clean fuel, its low energy density makes storage and transportation challenging. 16 CO_2 is a viable carrier for solar-generated H_2 ; 16,17 both the hydrogenation of CO_2 to formate 18 and the dehydrogenation of formic acid (HCOOH, FA) 19 are topical subfields in green-energy research. $^{10,20-22}$

Many effective catalysts for FA (de)hydrogenation are known, with turnover numbers (TONs) exceeding the millions. Several of these catalysts utilize precious metals, but robust examples with earth-abundant metals are also known. 16 Less common are examples of catalysts capable of both FA dehydrogenation and the reverse $\rm CO_2$ hydrogenation. $^{18d,23-31}$

Received: June 29, 2021 Revised: September 8, 2021 Published: October 18, 2021





This reversible catalysis is rarely achieved with base metals.³² The more challenging reaction, CO₂ hydrogenation, often requires high pressures of both CO₂ and H₂ and/or strong bases to achieve high TON.¹⁶ Significantly, we disclose here a Mo formate hydride complex that forms, at ambient temperature and atmospheric pressure, from CO₂ and H₂. This complex is demonstrated to serve as a precatalyst for both FA dehydrogenation and CO₂ hydrogenation. Stoichiometric studies inform reasonable operative mechanisms for each process, which are proposed to share a monohydride cation intermediate. Over 100 turnovers for both H₂ storage and release are achieved, both under basic conditions.

2. RESULTS AND DISCUSSION

2.1. Small-Molecule Binding and Activation Chemistry. We previously described the equilibrium binding of dihydrogen (H_2) and CO_2 in competition with dinitrogen (N_2) starting from complex 1 within the context of H_2 storage³³ and CO_2 reduction,³⁴ respectively (Scheme 1).

Scheme 1. Small-Molecule Binding Equilibria at Low-Valent Molybdenum

Under a H_2 atmosphere, the dinitrogen ligand of 1 is displaced, affording dihydride 2. This process is reversible, and complex 1 is regenerated when 2 is placed under N_2 . Similarly, an equilibrium between N_2 (1) and CO_2 (3) binding is established for this system, favoring the N_2 adduct except in the presence of Lewis acid additives. These findings support a relatively flat potential energy surface for small-molecule binding/exchange and suggest the possibility for an additional equilibrium between H_2 and CO_2 .

Placing intermediate dihydride complex **2** under one atmosphere of CO_2 afforded a mixture of **2** and **3**. With time, a new resonance was observed in the $^{31}P\{^1H\}$ NMR spectrum at 89.8 ppm. The addition of CO_2 (1 atm) and H_2 (ca. 4 atm) to **1** led to quantitative conversion to this new complex. The 1H NMR spectrum displayed a diagnostic low-field resonance at 8.9 ppm, consistent with CO_2 insertion and formation of formate hydride complex **4**. Section and formation of formate hydride complex **4**. While there were no high-field signals in the 1H NMR spectrum, an apparent triplet $(^2J(P,H) = 86.3 Hz)$ was observed at 1.9 ppm. This large scalar coupling and a weak correlation with the

central arene protons at 6.2 ppm (Figure S3) both support the assignment of this spectral feature to a hydride.

Complex 4 reverts to 1 under a N_2 atmosphere on the timescale of crystallization, inhibiting structural characterization of 4. However, a related complex, carboxylate hydride 5, can be prepared and crystallographically characterized. Treating Mo N_2 adduct 1 with 1 equiv of ${}^tBuC_6H_4C(O)OH$ in C_6H_6 confers quantitative conversion to carboxylate hydride 5 (Figure 1A). The spectroscopic signature of 5 closely

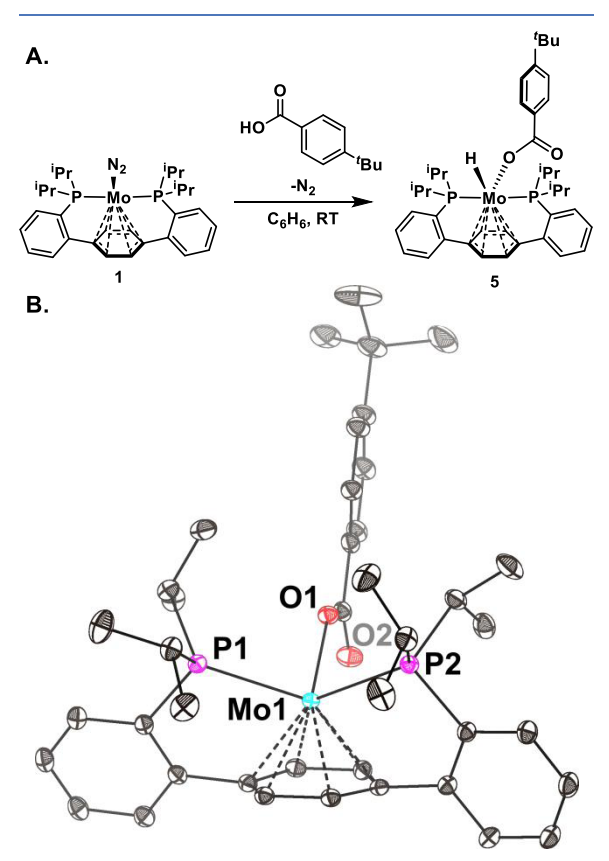


Figure 1. Synthesis (A) and solid-state structure (B) of carboxylate hydride complex **5.** Thermal anisotropic displacement ellipsoids are shown at a 50% probability level. Hydrogen atoms are omitted for clarity. Whereas the hydride is discernable in the Fourier map, we elect to omit it given the positional uncertainty resulting from hydrogen's low electron density. ⁴⁰ Selected bond distances [Å]: Mo₁–Carene(ave.): 2.266(2), Mo₁–O₁: 2.196(1), O₁–C₃1: 1.284(2), and C₃1–O₂: 1.237(2).

resembles that of **4**, with a hydride resonance at 2.1 ppm, showing a ${}^2J(P,H)$ scalar coupling of 90.7 Hz. The solid-state metrics for **5** are in accord with the structure inferred from solution spectroscopy; an η^6 Mo—arene interaction is observed with *trans*-spanning diphosphines and a κ^1 carboxylate (Figure 1B).

2.2. Silane Coordination Chemistry. While the formation of 4 represents the successful two-electron reduction of CO₂, we sought to liberate the formate fragment to facilitate further chemistry. Silanes have been shown to insert into metal formates, driven by the formation of a strong Si–O bond, with concomitant generation of a metal hydride. On the present

system, this sequence would regenerate complex 2, closing a catalytic cycle. Considering the deinsertion chemistry observed for 4 (vide supra), it is best formed in situ under a mixed atmosphere of CO_2 and H_2 . We therefore explored the reactivity of dinitrogen adduct 1 with silanes for comparison with H_2 .

The addition of silanes to electron-rich Mo complexes has been shown to result in Si–H bond activation chemistry, ^{38,39} a reactivity feature that holds true for 1 (Figure 2A). Treating a

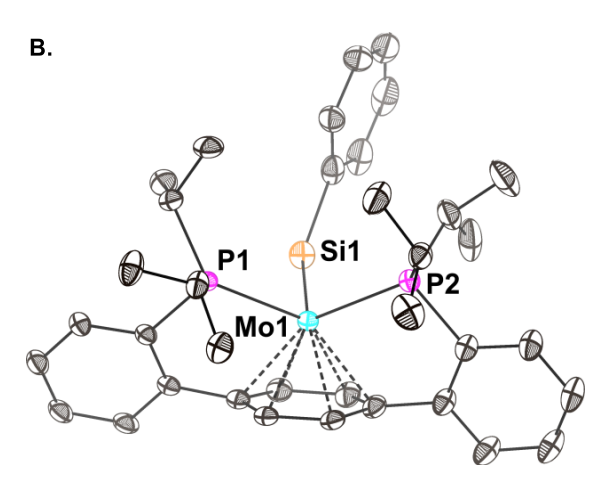


Figure 2. Synthesis (A) and solid-state structure (B) of silyl hydride complex **6.** Thermal anisotropic displacement ellipsoids are shown at a 50% probability level. Hydrogen atoms are omitted for clarity. Whereas the hydride is discernable in the Fourier map, we elect to omit it given the positional uncertainty resulting from hydrogen's low electron density. Selected bond distances [Å]: Mo1–Carene(ave.): 2.268(1) and Mo1–Si1: 2.5313(4).

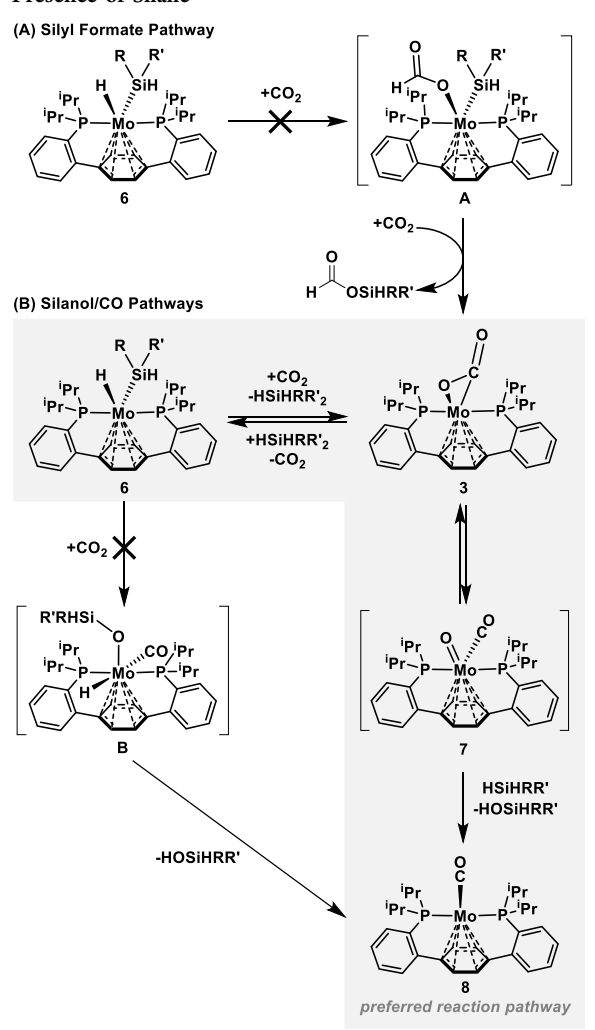
solution of 1 with PhSiH₃ leads to a lightening of the reaction mixture and effervescence, consistent with N₂ loss. The ¹H NMR spectrum shows both a highly shielded triplet ($^2J(P,H) = 43.6 \text{ Hz}$) at -3.13 ppm and a singlet at 5.51 ppm with clear 29 Si satellites ($^2J(^{29}\text{Si},H) = 166.34 \text{ Hz}$). The $^{31}P\{^{1}H\}$ NMR spectrum shows a single peak at 70.82 ppm. Combined, these spectroscopic features are consistent with the formulation of the product as phenylsilyl hydride 6, resulting from Si–H oxidative addition. Single crystals of 6 were obtained by cooling a concentrated hexanes solution to -35 °C, corroborating the proposed molecular structure (Figure 2B).

Reactions with secondary silanes demonstrate that the oxidative addition chemistry is sensitive to the steric environment at silicon. Addition of PhMeSiH₂ (1 equiv) afforded 40% conversion ($^{31}P^{\{1}H\}$ NMR integration) to 6'; adding excess silane (5 equiv) or degassing the reaction via sequential freeze–pump–thaw cycles resulted in the quantitative formation of the oxidative addition product 6' (Figure S11). The hydride resonance for 6' ($\delta = -3.32$ ppm) shows a smaller $^{2}J(P,H)$ scalar coupling constant (38.9 Hz), a

spectroscopic manifestation attributed to a more crowded coordination sphere and a contracted $\angle P1\text{-Mo1-P2}$. The tertiary silane, Et₃SiH, showed no reactivity with 1 even when present in 100-fold excess and after rigorous removal of N_2 from the headspace.

2.3. Carbon Dioxide Reduction with Silanes. With precedent for CO₂ insertion into the Mo—H bond of **2**, similar reactivity was sought from silyl hydride compounds (Scheme **2A**). Disappointingly, no reaction was observed upon treating

Scheme 2. Proposed CO_2 Reduction Mechanism in the Presence of Silane^a



^aProposed intermediates are designated with square brackets. The same putative C–O cleavage product, 7, is invoked in the absence of silane, leading to phosphine oxide formation and demetallation.

6 or 6' with 1 atm. of CO_2 (cf. 6 \rightarrow A, Scheme 2). Under more forcing conditions, heating to 70 °C for 12 h, a complex mixture of species results prior to the nearly quantitative formation of the previously reported molybdenum(0) carbonyl complex, 8 (Figure S15). Kinetic analysis of this C–O cleavage reaction showed substrate inhibition; from 1 to 5 equiv, added silane increased the rate of reaction (Figure S14). However,

higher silane concentration impeded the reaction, suggesting an abnormal CO_2 reduction mechanism (*vide infra*). While cooperative M/Si cleavage of CO_2 is known, $^{41-43}$ this reactivity would proceed from a Mo silyl complex and is therefore inconsistent with the observed inhibition (Scheme 2B, left). Additionally, increased steric bulk at silicon resulted in faster reactivity, with 6 forming 8 more slowly than 6', further supporting the premise that CO_2 reactivity requires silane dissociation.

A control reaction demonstrated that silane was superfluous to C-O cleavage chemistry. Heating a C₆D₆ solution of 3 afforded a mixture of 8 (56%), para-terphenyl diphosphine oxide (P2°; 17%), and free diphosphine (P2; 27%), as determined by relative integration of the 31P{1H} NMR spectrum (versus a PPh3 capillary standard). Heating isotopically labeled 3-13C provided 8-13C, as evidenced by 31P{1H} and 13C{1H} NMR spectroscopies, confirming the source of the CO unit. Though molybdenum CO2 complexes are known to undergo ligand redistribution reactions, providing carbonyl carbonate complexes from bound CO2, 44 the observations of both >50% conversion to 8 and phosphine oxide, P20, contradict this reactivity manifold. Phosphine-supported transition-metal CO2 adducts have been demonstrated to cleave CO₂ to the corresponding carbonyl complex and phosphine oxide, ^{19a,45} a reaction pathway that is more congruent with the observed experimental data.

But what is the fate of the cleaved O-atom in silane reactions? Oxygen atom transfer to silane seemed most likely, as no phosphine oxide was observed and conversion to 8 was effectively quantitative. Gas chromatography/mass spectrometry (GC/MS) analysis of the reaction mixture following heating 6' under CO₂ for 12 h demonstrated the formation of both phenyl methyl silanol as well as polysiloxanes, both of which were absent in the control (Figure S16).

At this juncture, two mechanisms seemed plausible, both involving Mo-mediated C-O cleavage to a Mo^{II} oxo complex that is subsequently reduced by silane (Scheme 2). A preequilibrium between silyl hydride and CO2 is consistent with the reaction kinetics; reversible oxidative addition of η^2 -Si-H bonds at Mo has precedent.³⁹ Bulky silanes favor the formation of 3, the species proposed to undergo C-O scission, while less sterically imposing silanes (and high silane concentrations), sequester Mo as unreactive 6. Relatively low PhMeSiH₂ concentrations increase the rate of formation of 8, supporting a silane-dependent rate affecting step. The initial equilibrium between silane oxidative addition and CO₂ binding (inverse order in [Si]), in conjunction with silane addition to the putative carbonyl oxo 7 (first order in [Si]), 12i,46 is consistent with the complex silane dependence observed in the reaction kinetics. In contrast, intermolecular reactivity, oxo trapping via molybdenum silyl hydride 6, is expected to be zeroth order in silane and second order in Mo, inconsistent with our findings. However, we cannot conclusively rule out intermolecular reactivity involving a Mo-mediated oxygen abstraction and downstream silylation of the resultant Mo(II) oxide. Notably, these pathways contrast reactivity established for Ir pincer complexes in which silyl formates are decarbonylated en route to an Ir-CO complex and silanol. 12d

2.4. Evidence for On-Metal C-O Cleavage. Additional evidence supporting an intramolecular pathway was provided by reactions with carbonyl sulfide (OCS). Placing a C_6D_6 solution of 1 under an atmosphere of OCS resulted in the immediate formation of an asymmetric complex, as demonstrated as the contract of the complex of the comp

strated by two coupling doublets (83.41 and 54.34 ppm, ${}^2J(P,P)=17.8$ Hz) in the ${}^{31}P\{{}^{1}H\}$ NMR spectrum. Upon standing, X-ray quality single crystals were obtained, evincing the formation of carbonyl phosphine sulfide complex 9 (Figure 3). The asymmetry in two chelating donors explains ${}^{31}P$ NMR

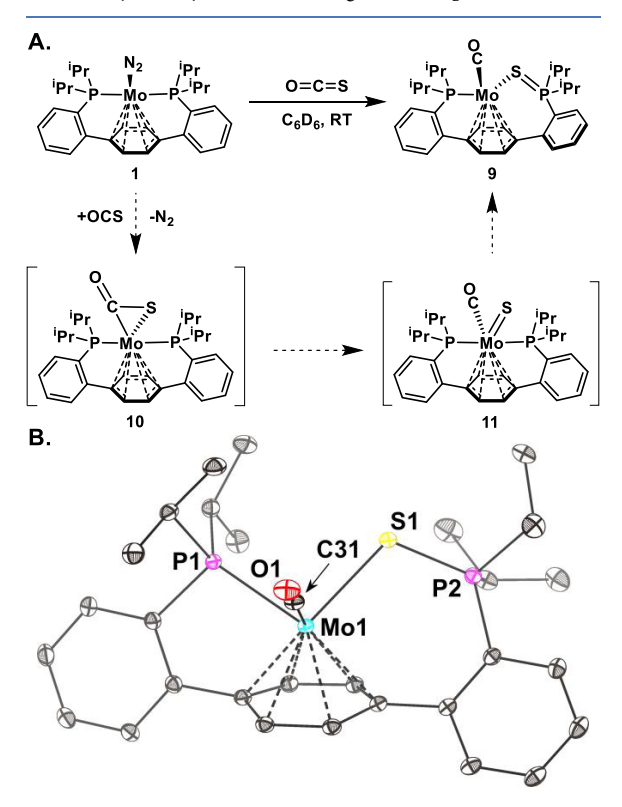


Figure 3. Synthesis (A) and solid-state structure (B) of **9.** In the reaction scheme, dashed arrows show a proposed pathway for the formation of **9** *via* putative intermediates **10** and **11** (square brackets). In the solid-state structure, thermal anisotropic displacement ellipsoids are shown at a 50% probability level. Hydrogen atoms are omitted for clarity. Selected bond distances [Å]: Mo1–S1: 2.5016(3) and S1–P2: 2.0053(4).

features. Compound 9 likely forms via initial cleavage of the more reactive C–S bond of OCS, giving a transient Mo carbonyl sulfide complex, 10. Oxidative cleavage of C=E multiple bonds has been demonstrated on W;^{47–49} a similar process is likely operative here. Analogously to the P–C bond formation reported from Mo^{II} methylidene complexes supported by this ancillary ligand,⁴⁷ the Mo^{II} sulfide afforded by C–S cleavage inserts into the Mo–P bond, giving the observed phosphine sulfide product. Under CO₂ reduction conditions, the oxo congener of sulfide 11 (cf. 7, Scheme 2) is proposed to oxidize silanes faster than the phosphine ligand, but in the absence of silanes, the oxygen congener of 9 is likely formed, leading ultimately to the observed decomposition to P2^O.

2.5. Carbon Dioxide Hydrogenation Catalysis. Stymied by unsuccessful conversion to free silyl formate using silanes, we investigated the potential of adding base to complex 4 in an attempt to exploit a thermodynamically viable route to dissociate formate anion. As amines are mild bases that render CO₂ hydrogenation exergonic, complex 4 was treated with 10

equiv of 1,8-diazabicyclo[5.4.0] undec-7-ene (DBU) under $\rm N_2$ (Scheme 3). No reaction was observed, even over the course of 24 h.

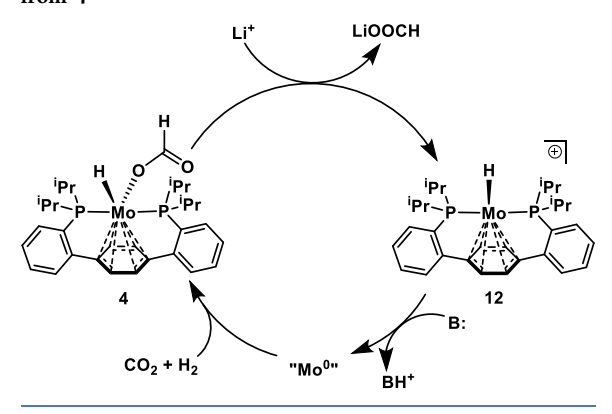
Scheme 3. Stoichiometric Reactions of 4 with Base (Top), Lewis Acid (Down), and Both (Diagonal)

Motivated by reports of Lewis acids (LAs) assisting in formate dissociation,³² alkali metal salts were screened as reaction additives. Addition of 10 equiv of LiOTf to 4 in C₆D₆ results in moderate conversion to a mixture of species, including 1, 3, and an unidentified product (Figure S21). This new complex, 12, bears a triplet with strong scalar coupling (2.27 ppm; ${}^{2}J(P,H) = 86.1 \text{ Hz})$ in its ${}^{1}H$ NMR spectrum, attributed to a Mo hydride, with corresponding central arene resonances at 4.21 and 3.94 ppm. Formulation of 12 as a hydride cation is further supported by independent synthesis; the same spectroscopic signature is observed when treating dinitrogen complex 1 with lutidinium trifluoromethane sulfonate (LutHOTf) in C₆D₆. Moreover, when acetonitrile is added to complex 12 synthesized from 1, the previously characterized acetonitrile adduct, 13, is formed quantitatively (Figure S22).33,50

While the generation of 12 corresponds to successful formate dissociation, monitoring LiOTf addition to 4 over 12 h showed less than 50% total conversion of the starting material. In contrast, treating a C_6D_6 solution of 4 with 10 equiv of both base (DBU) and LA (LiOTf) resulted in quantitative conversion to Mo⁰ complexes, 1 (86%) and 3 (14%), in just 30 min at room temperature (Figure S21).

These stoichiometric reactions map out a catalytic cycle for CO_2 hydrogenation to formate (Scheme 4). As a first step, LA-assisted formate dissociation gives Mo-hydride cation 12; 12 is observed in the stoichiometric reaction of 4 with LiOTf. Deprotonation of 12 affords a Mo(0) species, consistent with

Scheme 4. Plausible Catalytic Cycle for CO₂ Hydrogenation from 4



conversion of 4 to N_2 adduct 1 in the presence of both LiOTf and DBU under a dinitrogen atmosphere. Employing the additive ligand acidity constant equation of Morris, the p K_a of 12 can be estimated to be 18, in agreement with the proposed deprotonation with DBU (p $K_a^{\rm THF}$ [DBUH]⁺ \approx 20). S1 CO₂/H₂ addition and insertion, the initial synthetic route to access 4, closes the cycle.

Applying this mechanistic understanding to catalysis proved successful (Table 1). Utilization of strong lithium bases

Table 1. Reaction Optimization for Mo-Catalyzed CO_2 Hydrogenation

$$\begin{array}{c|c} \textbf{O} & 5 \ \mu \textbf{M} \ \textbf{1} \\ 0.5 \ mM \ base/additive} \\ \textbf{O} & \textbf{THF}, \ 70 \ ^{\circ}\text{C}, \ 20 \ h} \\ \hline \\ \textbf{entry} & \textbf{base/additive} \\ \textbf{1} & \textbf{DBU/NaOTf} & 1:1 & 6 \\ 2 & \textbf{LiHMDS} & 1:1 & 106 \\ \hline \end{array}$$

1:1

55

substantially increased the turnover number (TON) for formate generation with LiOtBu surpassing 50 turnovers and LiHMDS exceeding 100. 52 While these numbers are lower than those achieved in contemporary CO₂ hydrogenation catalyses, reactions operate at much lower pressures and outperform comparable molybdenum catalysts. 18th

2.6. Formic Acid Dehydrogenation Catalysis. To complete a reversible hydrogen storage cycle, coupled to two-electron CO2 reduction, requires the dehydrogenation of formic acid. Akin to the synthesis of carboxylate hydride 5, the direct reaction of dinitrogen adduct 1 with formic acid was expected to provide a route to 4, which has already been demonstrated to undergo decarboxylation (vide supra). Addition of 5 equiv of formic acid to complex 1 and subsequent heating (70 $^{\circ}$ C) resulted in complete consumption of the FA and generation of formate hydride compound 4. Heating a C₆D₆ solution of formate hydride 4 to 70 °C, in a sealed tube, afforded 85% conversion of the starting material to a mixture of N₂ adduct 1 (23%), CO₂ adduct 3 (19%), and H₂ complex 2 (40%) after 1 h (Figure S20). Though insertion of CO₂ into Mo-dihydride 2, is favored at room temperature, at higher temperature, deinsertion is entropically preferred, leading to reversion to the gaseous small molecules. However,

3

LiO^tBu

ACS Catalysis pubs.acs.org/acscatalysis

attempted catalysis with complex 1 in dioxane at 80 °C in an open system (i.e., eudiometer), demonstrated only slightly super stoichiometric reactivity for formic acid dehydrogenation (1.5 equiv; Table 2).

Table 2. Additive Optimization for FA Dehydrogenation Catalysis

O	0.1 mol% 1 10 mol% additive		O	+ H ₂
но Н	dioxane, 80	°C, time	0	. 112
entry	additive	time (h)		TON
1		1		3
2	LiCl	1		3
3	$B(C_6F_5)_3$	1		3
4	NaBAr ₂₄ ^{Fa}	1		3
5	NaBF ₄	1		0
6	NaOOCH	5		298
7	$DMAP^{b}$	3		196

^aBAr₂₄^F = tetrakis(3,5-bis(trifluoromethyl)phenyl)borate. ^bDMAP = N,N-dimethyl-4-aminopyridine.

DBU

Literature reports have disclosed profound LA effects on the activity of formic acid dehydrogenation catalysts. 19e The proposed mechanism invokes a LA-assisted formate decarboxylation step; the same elementary step presumed to be slow in the present system. Unfortunately, screening a sampling of Lewis acid additives proved unsuccessful, mirroring the activity of compound 1 alone (Table 2, Entries 2-5). Extending the reaction time resulted in no additional gas evolution, even in cases with (super)stoichiometric conversion (Table 2, Entries

1-4). Investigating sodium formate (NaOOCH), a postulated source of sodium cation, drastically improved formate dyhdrogenation, achieving almost 300 turnovers. Given the inefficacy of other sodium sources, the improved performance was deemed related to the Brönsted basicity. Other bases were explored, showing optimal activity with DBU (Table 2, Entry 8).

The present data support two distinct pathways for FA dehydrogenation (Scheme 5). An inefficient, but demonstrated, cycle involves thermal decarboxylation of 4 to a mixture of 2 and 3 (Scheme 5, right). As reported above, a decomposition pathway from CO2 adduct 3 is thermally induced C-O cleavage to monocarbonyl 8 with concomitant formation of phosphine oxide (P2O). If the rate of this process is comparable to that of deinsertion, it may explain the low TON observed in the absence of additives (vide supra); Mo complexes would ultimately be converted to inactive 8 (Figure S18). In a productive sense, both 2 and 3 could react with formic acid to return complex 4, closing the cycle.

The alternative pathway, which is hypothesized to be responsible for the higher turnover numbers observed in the presence of Brönsted bases, involves protonation of 4 to afford a formate cation (14; Figures S23 and S24). We cannot explicitly rule out a step-wise protonation/H2 reductive elimination from a Mo(IV) dihydride formate cation or a protonation, decarboxylation, H2 reductive elimination sequence invoking a Mo(IV) trihydride cation. This latter Mo(IV) species has been characterized on the para-terphenyl diphosphine ligand scaffold previously and readily loses H₂.³ Decarboxylation of 14 (or the aforementioned series of steps proceeding via Mo(IV) intermediates) would yield hydride cation 12, the same intermediate species proposed in CO2 hydrogenation above. Formate coordination regenerates 4, closing the catalytic cycle (Figure S25).

Scheme 5. Plausible Mechanisms for Formic Acid Dehydrogenation from 4^a

3.3

615

^aComplex 14 is proposed without any direct spectroscopic characterization—it has been designated as a putative intermediate with square brackets.

The role of basic additives is not immediately obvious, but all of the bases used are sufficiently strong to deprotonate formic acid. This would increase the solution concentration of formate anion, which may in turn aid turnover $(12 \rightarrow 4)$, if formate coordination is rate limiting. Alternatively, amine bases may act to provide a soluble source of formate, both keeping Mo intermediates from precipitating over the course of the reaction and aiding in the regeneration of 4. The catalytic conditions are run with excess formic acid such that protonation $(4 \rightarrow 14)$ would still be viable, even after the observed turnovers. A different mechanism involving deprotonation of 12 is not consistent with the lack of reactivity in the presence of a base under stoichiometric conditions.

3. CONCLUSIONS

Two modes of Mo-mediated CO_2 reduction have been presented. Stoichiometric reactions with silanes afford CO and silanol from CO_2 via a mechanism involving Mo-promoted intramolecular $\mathrm{C-O}$ bond cleavage and O-atom transfer to silane. Catalytic CO_2 hydrogenation proceeds in the presence of both a Lewis acid additive and base, affording respectable turnover numbers considering the low pressures of H_2 and CO_2 employed. The same species demonstrated to be catalytically competent for formate formation catalyzes the reverse reaction, formic acid dehydrogenation. The isolation of intermediates and studies of their reactivity have provided mechanistic insights into the divergent modes of CO_2 reduction at Mo.

ASSOCIATED CONTENT

Supporting Information

The Supporting Information is available free of charge at https://pubs.acs.org/doi/10.1021/acscatal.1c02922.

Detailed synthetic protocols, characterization data, spectroscopic data, and kinetic data.

Crystallographic data for 5, 6, and 9 (CIF)

General considerations; NMR spectra; silane coordination chemistry; CO_2 cleavage kinetics in the presence of PhMeSiH₂; GC/MS data; general procedures for catalytic reactions; stoichiometric reactivity targeting catalytic intermediates; and crystallographic information (PDF)

AUTHOR INFORMATION

Corresponding Author

Theodor Agapie — Division of Chemistry and Chemical Engineering, California Institute of Technology, Pasadena, California 91125, United States; ⊚ orcid.org/0000-0002-9692-7614; Email: agapie@caltech.edu

Authors

Joshua A. Buss — Division of Chemistry and Chemical Engineering, California Institute of Technology, Pasadena, California 91125, United States; Present Address: Department of Chemistry, University of Michigan, 930 North University Avenue, Ann Arbor, Michigan 48109, United States; orcid.org/0000-0002-3347-8583

Naoki Shida — Division of Chemistry and Chemical Engineering, California Institute of Technology, Pasadena, California 91125, United States; Present Address: Department of Chemistry and Life Science, Yokohama National University, 79-5 Tokiwadai, Hodogaya-ku, Yokohama, Kanagawa 240-8501, Japan. Tianyi He — Division of Chemistry and Chemical Engineering, California Institute of Technology, Pasadena, California 91125, United States; orcid.org/0000-0002-8191-188X

Complete contact information is available at: https://pubs.acs.org/10.1021/acscatal.1c02922

Author Contributions

 $^{\parallel}$ J.A.B. and N.S. contributed equally to this work.

Notes

The authors declare no competing financial interest.

ACKNOWLEDGMENTS

The authors thank Larry Henling and Mike Takase for crystallographic assistance and David VanderVelde for NMR expertise. The X-ray diffraction and NMR instrumentation were partially supported by the Dow Next Generation Educator Fund. T.A. is grateful for support from the NSF (CHE-1800501) for synthetic studies and DOE (Joint Center for Artificial Photosynthesis, Award Number DE-SC0004993) and King Fahd University of Petroleum and Minerals, Dhahran, Saudi Arabia (offered under the KFUPM-Caltech Research Collaboration) for CO₂ conversion studies. J.A.B. and N.S. are grateful for an NSF graduate research fellowship and a Grant-in-Aid for JSPS Research Fellows (No. 16J07350), respectively.

■ REFERENCES

- (1) Lewis, N. S.; Nocera, D. G. Powering the Planet: Chemical Challenges in Solar Energy Utilization. *Proc. Natl. Acad. Sci. U.S.A.* **2006**, *103*, 15729–15735.
- (2) National Research Council (US) Chemical Sciences Roundtable. Carbon Management: Implications for R&D in the Chemical Sciences and Technology: A Workshop Report to the Chemical Sciences Roundtable; National Academies Press: Washington, DC, 2001; p 5, Carbon Dioxide as a Feedstock. https://www.ncbi.nlm.nih.gov/books/NBK44146/.
- (3) Resasco, J.; Bell, A. T. Electrocatalytic CO₂ Reduction to Fuels: Progress and Opportunities. *Trends Chem.* **2020**, *2*, 825–836.
- (4) Zhang, X.; Fevre, M.; Jones, G. O.; Waymouth, R. M. Catalysis as an Enabling Science for Sustainable Polymers. *Chem. Rev.* **2018**, 118, 839–885.
- (5) Bontemps, S. Boron-Mediated Activation of Carbon Dioxide. Coord. Chem. Rev. 2016, 308, 117–130.
- (6) Fernández-Alvarez, F. J.; Aitani, A. M.; Oro, L. A. Homogeneous Catalytic Reduction of CO₂ with Hydrosilanes. *Catal. Sci. Technol.* 2014, 4, 611–624.
- (7) Zhang, Y.; Zhang, T.; Das, S. Catalytic Transformation of CO_2 into C_1 Chemicals Using Hydrosilanes as a Reducing Agent. *Green Chem.* **2020**, 22, 1800–1820.
- (8) Chen, J.; McGraw, M.; Chen, E. Y.-X. Diverse Catalytic Systems and Mechanistic Pathways for Hydrosilylative Reduction of CO₂. *ChemSusChem* **2019**, *12*, 4543–4569.
- (9) Olah, G. A.; Prakash, G. K. S.; Goeppert, A. Anthropogenic Chemical Carbon Cycle for a Sustainable Future. *J. Am. Chem. Soc.* **2011**, *133*, 12881–12898.
- (10) Wang, W.-H.; Himeda, Y.; Muckerman, J. T.; Manbeck, G. F.; Fujita, E. CO₂ Hydrogenation to Formate and Methanol as an Alternative to Photo- and Electrochemical CO₂ Reduction. *Chem. Rev.* **2015**, *115*, 12936–12973.
- (11) Kar, S.; Kothandaraman, J.; Goeppert, A.; Prakash, G. K. S. Advances in Catalytic Homogeneous Hydrogenation of Carbon Dioxide to Methanol. *J. CO₂ Util.* **2018**, 23, 212–218.

(12) For select recent references, see: (a) Koinuma, H.; Kawakami, F.; Kato, H.; Hirai, H. Hydrosilylation of Carbon Dioxide Catalysed by Ruthenium Complexes. J. Chem. Soc. Chem. Commun. 1981, 213. (b) Eisenschmid, T. C.; Eisenberg, R. The Iridium Complex Catalyzed Reduction of Carbon Dioxide to Methoxide by Alkylsilanes. Organometallics 1989, 8, 1822-1824. (c) Berkefeld, A.; Piers, W. E.; Parvez, M. Tandem Frustrated Lewis Pair/Tris(Pentafluorophenyl)-Borane-Catalyzed Deoxygenative Hydrosilylation of Carbon Dioxide. J. Am. Chem. Soc. 2010, 132, 10660-10661. (d) Park, S.; Bézier, D.; Brookhart, M. An Efficient Iridium Catalyst for Reduction of Carbon Dioxide to Methane with Trialkylsilanes. J. Am. Chem. Soc. 2012, 134, 11404-11407. (e) Sattler, W.; Parkin, G. Zinc Catalysts for On-Demand Hydrogen Generation and Carbon Dioxide Functionalization. J. Am. Chem. Soc. 2012, 134, 17462-17465. (f) Scheuermann, M. L.; Semproni, S. P.; Pappas, I.; Chirik, P. J. Carbon Dioxide Hydrosilylation Promoted by Cobalt Pincer Complexes. Inorg. Chem. 2014, 53, 9463-9465. (g) Nguyen, T. V. Q.; Yoo, W.-J.; Kobayashi, S. Effective Formylation of Amines with Carbon Dioxide and Diphenylsilane Catalyzed by Chelating Bis(TzNHC) Rhodium Complexes. Angew. Chem., Int. Ed 2015, 54, 9209-9212. (h) Julián, A.; Jaseer, E. A.; Garcés, K.; Fernández-Alvarez, F. J.; García-Orduña, P.; Lahoz, F. J.; Oro, L. A. Tuning the Activity and Selectivity of Iridium-NSiN Catalyzed CO2 Hydrosilylation Processes. Catal. Sci. Technol. 2016, 6, 4410-4417. (i) Mazzotta, M. G.; Xiong, M.; Abu-Omar, M. M. Carbon Dioxide Reduction to Silyl-Protected Methanol Catalyzed by an Oxorhenium Pincer PNN Complex. Organometallics 2017, 36, 1688-1691. (j) Rauch, M.; Parkin, G. Zinc and Magnesium Catalysts for the Hydrosilylation of Carbon Dioxide. J. Am. Chem. Soc. 2017, 139, 18162-18165. (k) Feng, G.; Du, C.; Xiang, L.; del Rosal, I.; Li, G.; Leng, X.; Chen, E. Y.-X.; Maron, L.; Chen, Y. Side Arm Twist on Zn-Catalyzed Hydrosilylative Reduction of CO₂ to Formate and Methanol Equivalents with High Selectivity and Activity. ACS Catal. 2018, 8, 4710-4718. (1) Hulla, M.; Laurenczy, G.; Dyson, P. J. Mechanistic Study of the N-Formylation of Amines with Carbon Dioxide and Hydrosilanes. ACS Catal. 2018, 8, 10619-10630. (m) Tüchler, M.; Gärtner, L.; Fischer, S.; Boese, A. D.; Belaj, F.; Mösch-Zanetti, N. C. Efficient CO2 Insertion and Reduction Catalyzed by a Terminal Zinc Hydride Complex. Angew. Chem., Int. Ed. 2018, 57, 6906-6909. (n) Zhang, Q.; Fukaya, N.; Fujitani, T.; Choi, J.-C. Carbon Dioxide Hydrosilylation to Methane Catalyzed by Zinc and Other First-Row Transition Metal Salts. Bull. Chem. Soc. Jpn. 2019, 92, 1945-1949. (o) Rauch, M.; Strater, Z.; Parkin, G. Selective Conversion of Carbon Dioxide to Formaldehyde via a Bis(Silyl)-Acetal: Incorporation of Isotopically Labeled C1 Moieties Derived from Carbon Dioxide into Organic Molecules. J. Am. Chem. Soc. 2019, 141, 17754-17762. (p) Bertini, F.; Glatz, M.; Stöger, B.; Peruzzini, M.; Veiros, L. F.; Kirchner, K.; Gonsalvi, L. Carbon Dioxide Reduction to Methanol Catalyzed by Mn(I) PNP Pincer Complexes under Mild Reaction Conditions. ACS Catal. 2019, 9, 632-639. (q) Sattler, W.; Shlian, D. G.; Sambade, D.; Parkin, G. Synthesis and Structural Characterization of Bis(2-Pyridylthio)(p-Tolylthio)Methyl Zinc Complexes and the Catalytic Hydrosilylation of CO2. Polyhedron 2020, 187, No. 114542. (r) Ghosh, D.; Kumar, G. R.; Subramanian, S.; Tanaka, K. More than Just a Reagent: The Rise of Renewable Organohydrides for Catalytic Reduction of Carbon Dioxide. ChemSusChem 2021, 14, 824-841. (s) Chang, K.; Del Rosal, I.; Zheng, X.; Maron, L.; Xu, X. Hydrosilylative Reduction of Carbon Dioxide by a Homoleptic Lanthanum Aryloxide Catalyst with High Activity and Selectivity. Dalton Trans. 2021, 50, 7804-7809.

- (13) For select examples with chromium group catalysts, see: (a) Pal, R.; Groy, T. L.; Bowman, A. C.; Trovitch, R. J. Preparation and Hydrosilylation Activity of a Molybdenum Carbonyl Complex That Features a Pentadentate Bis(Imino)Pyridine Ligand. *Inorg. Chem.* 2014, 53, 9357–9365. (b) Fuchs, J.; Irran, E.; Hrobárik, P.; Klare, H. F. T.; Oestreich, M. Si-H Bond Activation with Bullock's Cationic Tungsten(II) Catalyst: CO as Cooperating Ligand. *J. Am. Chem. Soc.* 2019, 141, 18845–18850.
- (14) Itagaki, S.; Yamaguchi, K.; Mizuno, N. Catalytic Synthesis of Silyl Formates with 1 atm of CO_2 and Their Utilization for Synthesis

- of Formyl Compounds and Formic Acid. J. Mol. Catal. A: Chem. 2013, 366, 347–352.
- (15) For one such example, see Ref 12e.
- (16) For a recent comprehensive review, see: Sordakis, K.; Tang, C.; Vogt, L. K.; Junge, H.; Dyson, P. J.; Beller, M.; Laurenczy, G. Homogeneous Catalysis for Sustainable Hydrogen Storage in Formic Acid and Alcohols. *Chem. Rev.* **2018**, *118*, 372–433.
- (17) Onishi, N.; Iguchi, M.; Yang, X.; Kanega, R.; Kawanami, H.; Xu, Q.; Himeda, Y. Development of Effective Catalysts for Hydrogen Storage Technology Using Formic Acid. *Adv. Energy Mater.* **2019**, *9*, No. 1801275.
- (18) For select recent references, see: (a) Inoue, Y.; Sasaki, Y.; Hashimoto, H. Synthesis of Formates from Alcohols, Carbon Dioxide, and Hydrogen Catalysed by a Combination of Group VIII Transition-Metal Complexes and Tertiary Amines. J. Chem. Soc. Chem. Commun. 1975, 718. (b) Inoue, Y.; Izumida, H.; Sasaki, Y.; Hashimoto, H. Catalytic Fixation of Carbon Dioxide to Formic Acid by Transition-Metal Complexes under Mild Conditions. Chem. Lett. 1976, 5, 863-864. (c) Himeda, Y.; Onozawa-Komatsuzaki, N.; Sugihara, H.; Kasuga, K. Recyclable Catalyst for Conversion of Carbon Dioxide into Formate Attributable to an Oxyanion on the Catalyst Ligand. J. Am. Chem. Soc. 2005, 127, 13118-13119. (d) Tanaka, R.; Yamashita, M.; Nozaki, K. Catalytic Hydrogenation of Carbon Dioxide Using Ir(III) Pincer Complexes. J. Am. Chem. Soc. 2009, 131, 14168-14169. (e) Schmeier, T. J.; Dobereiner, G. E.; Crabtree, R. H.; Hazari, N. Secondary Coordination Sphere Interactions Facilitate the Insertion Step in an Iridium(III) CO2 Reduction Catalyst. J. Am. Chem. Soc. 2011, 133, 9274-9277. (f) Langer, R.; Diskin-Posner, Y.; Leitus, G.; Shimon, L. J. W.; Ben-David, Y.; Milstein, D. Low-Pressure Hydrogenation of Carbon Dioxide Catalyzed by an Iron Pincer Complex Exhibiting Noble Metal Activity. Angew. Chem., Int. Ed. 2011, 50, 9948-9952. (g) Zhang, Y.; MacIntosh, A. D.; Wong, J. L.; Bielinski, E. A.; Williard, P. G.; Mercado, B. Q.; Hazari, N.; Bernskoetter, W. H. Iron Catalyzed CO₂ Hydrogenation to Formate Enhanced by Lewis Acid Co-Catalysts. Chem. Sci. 2015, 6, 4291-4299. (h) Zhang, Y.; Williard, P. G.; Bernskoetter, W. H. Synthesis and Characterization of Pincer-Molybdenum Precatalysts for CO2 Hydrogenation. Organometallics 2016, 35, 860-865. (i) Vollmer, M. V.; Ye, J.; Linehan, J. C.; Graziano, B. J.; Preston, A.; Wiedner, E. S.; Lu, C. C. Cobalt-Group 13 Complexes Catalyze CO2 Hydrogenation via a Co(-I)/Co(I) Redox Cycle. ACS Catal. 2020, 10, 2459-2470. (19) For select recent references, see: (a) Shin, J. H.; Churchill, D. G.; Parkin, G. Carbonyl Abstraction Reactions of Cp*Mo(PMe₃)₃H with CO₂, (CH₂O)_n, HCO₂H, and MeOH: The Synthesis of Cp*Mo(PMe₃)₂(CO)H and the Catalytic Decarboxylation of Formic Acid. J. Organomet. Chem. 2002, 642, 9-15. (b) Loges, B.; Boddien, A.; Junge, H.; Beller, M. Controlled Generation of Hydrogen from Formic Acid Amine Adducts at Room Temperature and Application in H₂/O₂ Fuel Cells. Angew. Chem., Int. Ed. 2008, 47, 3962-3965. (c) Fellay, C.; Dyson, P. J.; Laurenczy, G. A Viable Hydrogen-Storage System Based on Selective Formic Acid Decomposition with a Ruthenium Catalyst. Angew. Chem., Int. Ed. 2008, 47, 3966-3968. (d) Boddien, A.; Mellmann, D.; Gärtner, F.; Jackstell, R.; Junge, H.; Dyson, P. J.; Laurenczy, G.; Ludwig, R.; Beller, M. Efficient Dehydrogenation of Formic Acid Using an Iron Catalyst. Science 2011, 333, 1733-1736. (e) Bielinski, E. A.; Lagaditis, P. O.; Zhang, Y.; Mercado, B. Q.; Würtele, C.; Bernskoetter, W. H.; Hazari, N.; Schneider, S. Lewis Acid-Assisted Formic Acid Dehydrogenation Using a Pincer-Supported Iron Catalyst. J. Am. Chem. Soc. 2014, 136, 10234-10237. (f) Celaje, J. J. A.; Lu, Z.; Kedzie, E. A.; Terrile, N. J.; Lo, J. N.; Williams, T. J. A Prolific Catalyst for Dehydrogenation of Neat Formic Acid. Nat. Commun. 2016, 7, No. 11308.
- (20) Jessop, P. G.; Joó, F.; Tai, C.-C. Recent Advances in the Homogeneous Hydrogenation of Carbon Dioxide. *Coord. Chem. Rev.* **2004**, 248, 2425–2442.
- (21) Wang, W.; Wang, S.; Ma, X.; Gong, J. Recent Advances in Catalytic Hydrogenation of Carbon Dioxide. *Chem. Soc. Rev.* **2011**, 40, 3703–3727.

- (22) Mellmann, D.; Sponholz, P.; Junge, H.; Beller, M. Formic Acid as a Hydrogen Storage Material Development of Homogeneous Catalysts for Selective Hydrogen Release. *Chem. Soc. Rev.* **2016**, 45, 3954–3988.
- (23) Papp, G.; Csorba, J.; Laurenczy, G.; Joó, F. A Charge/Discharge Device for Chemical Hydrogen Storage and Generation. *Angew. Chem., Int. Ed.* **2011**, *50*, 10433–10435.
- (24) Boddien, A.; Gärtner, F.; Federsel, C.; Sponholz, P.; Mellmann, D.; Jackstell, R.; Junge, H.; Beller, M. CO₂-"neutral" Hydrogen Storage Based on Bicarbonates and Formates. *Angew. Chem., Int. Ed.* **2011**, *50*, 6411–6414.
- (25) Hull, J. F.; Himeda, Y.; Wang, W.-H.; Hashiguchi, B.; Periana, R.; Szalda, D. J.; Muckerman, J. T.; Fujita, E. Reversible Hydrogen Storage Using CO₂ and a Proton-Switchable Iridium Catalyst in Aqueous Media under Mild Temperatures and Pressures. *Nat. Chem.* 2012, 4, 383–388.
- (26) Hsu, S.-F.; Rommel, S.; Eversfield, P.; Muller, K.; Klemm, E.; Thiel, W. R.; Plietker, B. A Rechargeable Hydrogen Battery Based on Ru Catalysis. *Angew. Chem., Int. Ed.* **2014**, *53*, 7074–7078.
- (27) Kothandaraman, J.; Czaun, M.; Goeppert, A.; Haiges, R.; Jones, J.-P.; May, R. B.; Prakash, G. K. S.; Olah, G. A. Amine-Free Reversible Hydrogen Storage in Formate Salts Catalyzed by Ruthenium Pincer Complex without PH Control or Solvent Change. *ChemSusChem* **2015**, *8*, 1442–1451.
- (28) Geri, J. B.; Ciatti, J. L.; Szymczak, N. K. Charge Effects Regulate Reversible CO₂ Reduction Catalysis. *Chem. Commun.* **2018**, 54, 7790–7793.
- (29) Semwal, S.; Kumar, A.; Choudhury, J. Iridium—NHC-Based Catalyst for Ambient Pressure Storage and Low Temperature Release of H₂ via the CO₂/HCO₂H Couple. *Catal. Sci. Technol.* **2018**, 8, 6137–6142.
- (30) Fidalgo, J.; Ruiz-Castañeda, M.; García-Herbosa, G.; Carbayo, A.; Jalón, F. A.; Rodríguez, A. M.; Manzano, B. R.; Espino, G. Versatile Rh- and Ir-Based Catalysts for CO₂ Hydrogenation, Formic Acid Dehydrogenation, and Transfer Hydrogenation of Quinolines. *Inorg. Chem.* **2018**, *57*, 14186–14198.
- (31) Kanega, R.; Ertem, M. Z.; Onishi, N.; Szalda, D. J.; Fujita, E.; Himeda, Y. CO₂ Hydrogenation and Formic Acid Dehydrogenation Using Ir Catalysts with Amide-Based Ligands. *Organometallics* **2020**, 39, 1519–1531.
- (32) Bernskoetter, W. H.; Hazari, N. Reversible Hydrogenation of Carbon Dioxide to Formic Acid and Methanol: Lewis Acid Enhancement of Base Metal Catalysts. *Acc. Chem. Res.* **2017**, *50*, 1040–1058
- (33) Buss, J. A.; Edouard, G. A.; Cheng, C.; Shi, J.; Agapie, T. Molybdenum Catalyzed Ammonia Borane Dehydrogenation: Oxidation State Specific Mechanisms. *J. Am. Chem. Soc.* **2014**, *136*, 11272–11275.
- (34) Buss, J. A.; VanderVelde, D. G.; Agapie, T. Lewis Acid Enhancement of Proton Induced CO₂ Cleavage: Bond Weakening and Ligand Residence Time Effects. *J. Am. Chem. Soc.* **2018**, *140*, 10121–10125.
- (35) Brower, D. C.; Winston, P. B.; Tonker, T. L.; Templeton, J. L. Bidentate and Unidentate Formato Ligands in Dicarbonylbis-(Formato)Bis(Triethylphosphine)Molybdenum. *Inorg. Chem.* 1986, 25, 2883–2888.
- (36) Fong, L. K.; Fox, J. R.; Cooper, N. J. Reactions of Carbon Dioxide with the Electron-Rich Polyhydride Complex [Mo-(dmpe)₂H₄]. Organometallics 1987, 6, 223–231.
- (37) Neary, M. C.; Parkin, G. Dehydrogenation, Disproportionation and Transfer Hydrogenation Reactions of Formic Acid Catalyzed by Molybdenum Hydride Compounds. *Chem. Sci.* **2015**, *6*, 1859–1865. (38) Luo, X.-L.; Kubas, G. J.; Burns, C. J.; Bryan, J. C.; Unkefer, C. J. Synthesis of the First Examples of Transition Metal η²-SiH₄ Complexes, Cis-Mo(η²-SiH₄)(CO)(R₂PC₂H₄PR₂)₂, and Evidence for an Unprecedented Tautomeric Equilibrium between an η²-SiH₄ Complex and a Hydridosilyl Species: A Model for Methane Coordination and Activation. *J. Am. Chem. Soc.* **1995**, *117*, 1159–

- (39) Zuzek, A. A.; Parkin, G. Si–H and Si–C Bond Cleavage Reactions of Silane and Phenylsilanes with Mo(PMe₃)₆: Silyl, Hypervalent Silyl, Silane, and Disilane Complexes. *J. Am. Chem. Soc.* **2014**, *136*, 8177–8180.
- (40) Bau, R.; Teller, R. G.; Kirtley, S. W.; Koetzle, T. F. Structures of Transition-Metal Hydride Complexes. *Acc. Chem. Res.* **1979**, *12*, 176–182
- (41) Whited, M. T.; Zhang, J.; Conley, A. M.; Ma, S.; Janzen, D. E.; Kohen, D. Bimetallic, Silylene-Mediated Multielectron Reductions of Carbon Dioxide and Ethylene. *Angew. Chem., Int. Ed.* **2021**, *60*, 1615–1619
- (42) Whited, M. T.; Zhang, J.; Donnell, T. M.; Eng, V. H.; Peterson, P. O.; Trenerry, M. J.; Janzen, D. E.; Taylor, B. L. H. Cooperative CO₂ Scission by Anomalous Insertion into a Rh–Si Bond. *Organometallics* **2019**, *38*, 4420–4432.
- $(\tilde{4}3)$ Whited, M. T.; Zhang, J.; Ma, S.; Nguyen, B. D.; Janzen, D. E. Silylene-Assisted Hydride Transfer to CO_2 and CS_2 at a $[P_2Si]Ru$ Pincer-Type Complex. *Dalton Trans.* **2017**, *46*, 14757–14761.
- (44) Alvarez, R.; Atwood, J. L.; Carmona, E.; Perez, P. J.; Poveda, M. L.; Rogers, R. D. Formation of Carbonyl-Carbonate Complexes of Molybdenum by Reductive Disproportionation of Carbon Dioxide. X-Ray Structure of $Mo_4(\mu_4\text{-CO}_3)(CO)_2(O)_2(\mu_2\text{-O})_2(\mu_2\text{-OH})_4(PMe_3)_6$. *Inorg. Chem.* **1991**, *30*, 1493–1499.
- (45) Anderson, J. S.; Iluc, V. M.; Hillhouse, G. L. Reactions of CO_2 and CS_2 with 1,2-Bis(Di-Tert-Butylphosphino)Ethane Complexes of Nickel(0) and Nickel(1). *Inorg. Chem.* **2010**, *49*, 10203–10207.
- (46) Nolin, K. A.; Krumper, J. R.; Pluth, M. D.; Bergman, R. G.; Toste, F. D. Analysis of an Unprecedented Mechanism for the Catalytic Hydrosilylation of Carbonyl Compounds. *J. Am. Chem. Soc.* **2007**, *129*, 14684–14696.
- (47) Bryan, J. C.; Geib, S. J.; Rheingold, A. L.; Mayer, J. M. Oxidative Addition of Carbon Dioxide, Epoxides, and Related Molecules to WCl₂(PMePh₂)₄ Yielding Tungsten(IV) Oxo, Imido, and Sulfido Complexes. Crystal and Molecular Structure of W(O)Cl₂(CO)(PMePh₂)₂. J. Am. Chem. Soc. 1987, 109, 2826–2828. (48) Bryan, J. C.; Mayer, J. M. Oxidative Addition of Carbon-Oxygen and Carbon-Nitrogen Double Bonds to WCl₂(PMePh₂)₄. Synthesis of Tungsten Metallaoxirane and Tungsten Oxo- and Imido-Alkylidene Complexes. J. Am. Chem. Soc. 1990, 112, 2298–2308.
- (49) Buss, J. A.; Bailey, G. A.; Oppenheim, J.; VanderVelde, D. G.; Goddard, W. A.; Agapie, T. CO Coupling Chemistry of a Terminal Mo Carbide: Sequential Addition of Proton, Hydride, and CO Releases Ethenone. *J. Am. Chem. Soc.* **2019**, *141*, 15664–15674.
- (50) This acetonitrile solvated species is not a competent precatalyst for FA dehydrogenation.
- (51) Morris, R. H. Brønsted–Lowry Acid Strength of Metal Hydride and Dihydrogen Complexes. *Chem. Rev.* **2016**, *116*, 8588–8654. Note: Using Morris' LAC equation and assuming the conjugate base is a five-coordinate Mo(0) species (i.e. no N₂ bound), the p K_a of the hydride cation was estimated as follows: $(8[ArR_2P \times 2] + 2.1[\eta^6 C_6H_6] + 2[Mo is 5d] + 6[\Delta coord. #]) = 18.2.$
- (52) Jeletic, M. S.; Mock, M. T.; Appel, A. M.; Linehan, J. C. A Cobalt-Based Catalyst for the Hydrogenation of CO₂ under Ambient Conditions. *J. Am. Chem. Soc.* **2013**, *135*, 11533–11536.